DTU Library

Description of the KLL Auger–Meitner decay spectra of argon following primary and satellite core-ionized states

Pedersen, Jacob; Decleva, Piero; Coriani, Sonia; Tenorio, Bruno Nunes Cabral

Link back to DTU Orbit

Description of the *KLL* Auger–Meitner decay spectra of argon following primary and satellite core-ionized states

Jacob Pedersen ; Piero Decleva ; Sonia Coriani ; Bruno Nunes Cabral Tenorio

View Online

Export Citation

CrossMark

The Journal of Chemical Physics

Special Topic: Adhesion and Friction

Submit Today!

Description of the *KLL* Auger–Meitner decay spectra of argon following primary and satellite core-ionized states

View Online   Export Citation   CrossMark

Jacob Pedersen,[1] [iD] Piero Decleva,[2] [iD] Sonia Coriani,[1,a] [iD] and Bruno Nunes Cabral Tenorio[1,a] [iD]

AFFILIATIONS

[1] DTU Chemistry–Department of Chemistry, Technical University of Denmark, Kemitorvet Bldg. 207,
DK-2800 Kongens Lyngby, Denmark
[2] Istituto Officina dei Materiali IOM-CNR and Dipartimento di Scienze Chimiche e Farmaceutiche,
Università degli Studi di Trieste, I-34121 Trieste, Italy

[a] Author to whom correspondence should be addressed: soco@kemi.dtu.dk and brncat@dtu.dk

ABSTRACT

The *K*-edge photoelectron and *KLL* Auger–Meitner decay spectra of Argon have been investigated computationally at the restricted active space perturbation theory to the second order level using biorthonormally transformed orbital sets. Binding energies were computed for the Ar 1*s* primary ionization, as well as for satellite states originated from shake-up and shake-off processes. Based on our calculations, the contributions of shake-up and shake-off states to the *KLL* Auger–Meitner spectra of Argon have been completely elucidated. Our results are compared with recent state-of-the-art experimental measurements on Argon.

I. INTRODUCTION

Auger–Meitner[1] or molecular Auger electron spectroscopy[2,3] is the study of autoionization mechanisms, i.e., electron emission following initial core excitation or core ionization of some atomic or molecular system. The technique offers crucial insight into the electronic structure of the probed system and provides an avenue for probing molecular dynamics such as relaxation pathways or decay channels.[2,3] The availability of such detailed information is expected to be paramount for advancements in several research areas, such as artificial photosynthesis, where it can be utilized to tune and tailor the functionality of solar batteries.[4–7]

Auger electron spectroscopy is commonly employed in cooperation with other x-ray spectroscopies, such as x-ray absorption spectroscopy (XAS) and x-ray photoelectron spectroscopy (XPS).[8–13] The manifestation of satellite states in photoelectron spectra is direct evidence of electronic correlation. In particular, satellite states originate from additional bound excitation or ionization subsequent to the initial core photoionization; therefore, satellite states

should not be visible in the photoelectron spectrum according to Koopmans' theorem. The breakdown of this single electron picture unambiguously illustrates the effect of electronic correlation.[14–16]

The satellite structures in the *KLL* Auger decay spectrum of Argon have previously been assigned in several experimental and theoretical studies.[17–30] In the most recent experimental study by Püttner *et al.*,[31] three different photon energies for measuring the Auger spectra were used, namely *hv* = 3216, 3400, and 4500 eV, which allowed the authors to distinguish between the shake transitions in both the ionization and the Auger decay.[31] Their assignments were mainly based on fit analyses and estimated energies of the final states from relativistic configuration interaction calculations. However, the authors concluded that much more sophisticated computations are required for an ultimate assignment of the experimental features.[31]

Typically, satellite processes are distinguished with respect to the mechanism entailing the transition. Most satellites are associated with correlation within the bound states. In the case of deep core holes, a major effect is the shrinking of the outer orbitals in

response to the core hole formation, i.e., electronic relaxation, which can be considered a special type of correlation. The corresponding effects are often called *shake* or *monopole* transitions and conserve the symmetry of the orbitals. Additional correlations may generate more complex multielectron transitions. Now, depending on the transition character, i.e., excitation or ionization, the shake transition is denoted *shake-up* or *shake-off*, respectively. In relation to the *K*-shell photoionization of Argon, the shake-up satellite thus corresponds to an additional bound excitation of *M*-shell electrons, whereas the shake-off satellite represents the doubly ionized final state.[25,32–35] Different mechanisms for the appearance of additional satellites, with symmetry changes, are the *conjugate* transitions, in which a dipole transition occurs within the bound states, and inter-channel coupling among different continua. One can also say that the satellite can result from a momentary interaction between the outgoing electron from the initial core ionization and some valence electron. The outgoing electron will interact and exchange energy and angular momentum with the valence electrons under its ejection trajectory, and satellite processes originating from this mechanism are called *knock* transitions.[31] In our analysis, however, we neglect knock processes, since shake processes are dominant over knock processes with respect to the formation of satellite structures, as demonstrated by Püttner *et al.*[31]

The underlying core-hole states of interest in this work and their respective Auger decay pathways are schematically represented in Fig. 1.

The calculation of Auger decay rates is an intricate task as it requires the computation of bound-continuum matrix elements. In particular, the description of the continuum is a strenuous computational effort, since the continuum cannot be built from the same square-integrable basis functions as the bound states.[36–38] This most often means that specialized software interfaced with general quantum chemistry software packages is required for proper treatment of the continuum.[39,40] Recent advances within the field include the Feshbach–Fano approach developed by Skomorowski and Krylov,[41] the spherical continuum-based methods of Inhester *et al.*,[42] and of Grell *et al.*,[43,44] and the complex-variable coupled cluster method proposed by Matz and Jagau.[45] Alternatively, multicentric B-splines can be used for a full description of the continuum.[46]

Our recent implementation,[47] on the other hand, is based on the one-center approximation (OCA) and relies on a restricted active space perturbation theory to second order (RASPT2) wave function parameterization of the bound states. The essence of OCA is the utilization of pre-calculated one-center two-electron integrals instead of the exact two-electron bound-continuum integrals.[47] This OCA-RASPT2 method has been utilized with success for the calculation of Auger spectra for small and medium size molecules.[8,47,48] The approach can also be employed to elucidate the Auger spectrum of atomic systems, as demonstrated for Neon in Ref. [47] and now for Argon in this study.

The OCA-RASPT2 protocol takes advantage of the state interaction approximation.[49] In particular, the core and valence orbitals utilized to produce, respectively, the initial and final bound states, are obtained from separate self-consistent field calculations followed by a biorthogonalization procedure. An impartial parameterization of the initial and final states is thereby obtained, in which a proper
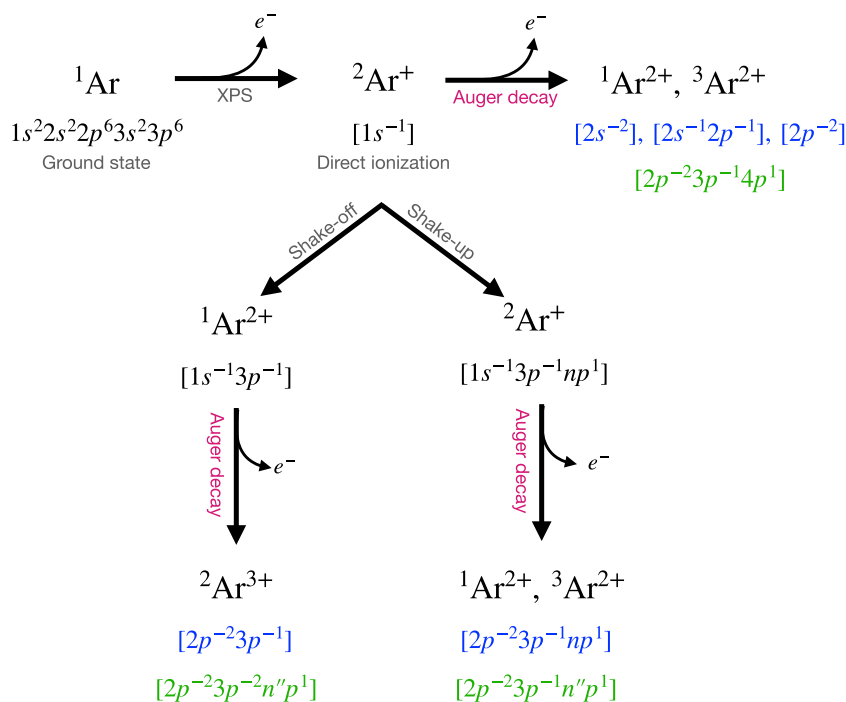
FIG. 1. Schematic representation of the main Auger decay pathways of core-ionized states $^{M_S}\mathrm{Ar}^N$, where $M_S = 2S + 1$ and N represent, respectively, the spin multiplicity and the charge. We used blue to highlight direct Auger-decay final states, and green for shake transitions during Auger decay.

account for the correlation effects responsible for the shake-up satellites is ensured.[50]

II. THEORY

A. Dyson orbitals within the RASSI approach

In Ref. [51], we presented a formalism to compute Dyson orbitals from a biorthonormal orbital set within the restricted active space state-interaction (RASSI) approach[49,52] for RASSCF/RASPT2 wave functions, as implemented in the OPENMOLCAS program package.[53]

Dyson orbitals are one-electron functions of great practical utility in describing molecular ionization processes and photoelectron spectroscopy.[54–59] Defined as overlaps between an initial N-electron wave function, Ψ_I^N, and a final $(N-1)$-electron wave function, Ψ_F^{N-1},

$$\phi_{IF}^d(x_1) = \sqrt{N} \int \Psi_F^{N-1}(x_2, \ldots, x_N) \Psi_I^N \times (x_1, x_2, \ldots, x_N)\, dx_2 \ldots dx_N, \quad (1)$$

they quantify the difference between the N-electron and $(N-1)$-electron systems upon electron detachment [or electron attachment when the $(N-1)$ wave function is the initial state].[58] As pointed out by Krylov,[59] the Dyson orbital can be thought of as the initial state of the ejected electron.

Within the RASSI formalism,[49,52] for a non-orthonormal pair of states, the Dyson orbital can be written as

$$\phi_{IF}^d = \sum_q \gamma_q^{IF} \widetilde{\phi}_q^I, \quad (2)$$

that is, as a linear combination of a biorthonormally transformed spin-orbital set of the initial wave function $\{\widetilde{\phi}^I\}$. The expansion coefficients in Eq. (2) are given by[39,54,55]

$$\gamma_q^{IF} = \langle \Psi_F^{N-1} | \hat{a}_q \Psi_I^N \rangle, \quad (3)$$

with the annihilation operator $\hat{a}_q$ being defined on the space of the biorthonormally transformed spin-orbitals $\{\widetilde{\phi}^I\}$ of Ψ_I^N. For later convenience, we also express the Dyson orbital in terms of its normalized counterpart, $\bar{\phi}_{IF}^d$, i.e.,

$$\phi_{IF}^d = |\phi_{IF}^d| \, \bar{\phi}_{IF}^d, \quad (4)$$

where the squared norm is, in the biorthonormal orbital basis, given by

$$|\phi_{IF}^d|^2 = \sum_{p,q} \gamma_p^{IF\star} \langle \widetilde{\phi}_p^I | \widetilde{\phi}_q^I \rangle \gamma_q^{IF}. \quad (5)$$

Considering a single-channel approximation of the final-state wave function,[60] the photoelectron matrix element $D_{Elm,\lambda}^{IF}$ can be written as[39,40,61]

$$D_{Elm,\lambda}^{IF} = \langle \phi_{Elm} | \vec{\mu}_\lambda | \phi_{IF}^d \rangle = |\phi_{IF}^d| \, \langle \phi_{Elm} | \vec{\mu}_\lambda | \bar{\phi}_{IF}^d \rangle, \quad (6)$$

where ϕ_{IF}^d is the Dyson orbital relative to the initial and final states of interest defined in Eq. (2), and ϕ_{Elm} is the wave function of the

ejected photoelectron; $\vec{\mu}_\lambda$ is the λ cartesian component of the electric dipole moment operator.

The photoelectron matrix element in the angular momentum (Elm) representation is transformed to the linear momentum $(\vec{k})$ representation, i.e., $D_{Elm,\lambda}^{IF} \rightarrow D_{\vec{k}\lambda}^{IF}$, in order to compute the molecular differential photoionization cross section,

$$\frac{d\sigma}{d\vec{k}} = 4\pi^2 \alpha \omega |D_{\vec{k}\lambda}^{IF}|^2, \quad (7)$$

where α is the fine structure constant, ω is the photon energy, and $\vec{k}$ is the momentum of the photoelectron in the molecular frame.[60]

Frequently, the sudden approximation[27] (SA) is applied to calculate the transition dipole matrix element in Eq. (7) at high kinetic energies. This approximation neglects the kinetic energy dependence of the transition strength, assuming that the dipole matrix element involving the continuum and the normalized Dyson orbital is almost independent on the final state F. This allows us to write

$$|D_{\vec{k}\lambda}^d|^2 \propto |\phi_{IF}^d|^2 = \sum_{p,q} \gamma_p^{IF\star} \langle \widetilde{\phi}_p^I | \widetilde{\phi}_q^I \rangle \gamma_q^{IF}. \quad (8)$$

The squared norms of Dyson orbitals are often called *spectral strengths* or *pole strengths*. Here, we use "pole strength" every time we are referring to squared norms of Dyson orbitals. The pole strengths R_I are in the following used as the intensities in the simulation of the XPS spectra.

B. Auger decay rates within the RASSI approach

The transition probability per unit time (transition rate) of Auger decay processes can be described by the Fermi golden rule.[62,63] In particular, the transition may occur from a core-excited (N-electron) initial state into a singly ionized [$(N-1)$-electron] final state, or from a core-ionized [$(N-1)$-electron] initial state into a doubly ionized [$(N-2)$-electron] final state. These two mechanisms are exploited in resonant Auger electron spectroscopy (RAES) and normal, or non-resonant, Auger electron spectroscopy (AES), respectively. Consequently, both decay processes entail the ejection of an Auger electron.[2]

The initial-state preparation (core-excitation or core-ionization) and the subsequent Auger decay are decoupled under the Wentzel approximation and can thereby be treated independently.[63,64] In the following, only the decay process will be explicitly considered.

The partial decay rate $\Gamma_{IF;\vec{k}}$ is given by the Wentzel ansatz,[64]

$$\Gamma_{IF;\vec{k}} = 2\pi \left| \langle \Psi_{F;\vec{k}} | \hat{H} - E_I | \Psi_I \rangle \right|^2. \quad (9)$$

Here, $\Psi_{F;\vec{k}}$ represents the wave function of the final state, $\hat{H}$ is the molecular Hamiltonian, and E_I is the eigenvalue corresponding to the energy of the initial-state wave function Ψ_I. Within the single-channel approximation, the final-state wave function is an antisymmetrized product of a bound-state $(N-1)$-electron wave function, Ψ_F^{N-1}, and a continuum orbital $\phi_{\vec{k}}$ with momentum $\vec{k}$,[8,47]

$$\Psi_{F;\vec{k}} = \mathscr{A}(\Psi_F^{N-1} \phi_{\vec{k}}). \quad (10)$$

To get the total partial decay rate, and thus the Auger intensity, or decay width, the partial decay rate must be integrated over all directions of the electron emission,

$$\Gamma_{IF} = \int d\vec{k}\ \Gamma_{IF;\vec{k}} = \sum_{l,m} \Gamma_{IF;Elm}, \quad (11)$$

where the continuum orbital has been transformed in the basis of angular momentum eigenstates in the second step, and an isotropic angular distribution of electron emission is assumed. Thereby, the integral reduces to a sum over the quantum numbers l and m that represent the angular momentum of the partial wave. Notice, moreover, that E is the kinetic energy of the continuum electron.[8,47]

The bound state and continuum orbitals are assumed orthogonal; therefore, the partial decay rate in terms of angular momentum eigenstates can be written as[43,47]

$$\Gamma_{IF;Elm} = 2\pi |A_{FI;Elm} + B_{FI;Elm}|^2, \quad (12)$$

with the Auger decay matrix elements

$$A_{IF;Elm} = \langle \hat{a}^\dagger_{Elm} \Psi^{N-1}_F | \hat{h} | \Psi^N_I \rangle = \sum_p \langle \phi_{Elm} | \hat{h} | \phi_p \rangle \gamma^{IF}_p, \quad (13)$$

and

$$B_{IF;Elm} = \langle \hat{a}^\dagger_{Elm} \Psi^{N-1}_F | \hat{g} | \Psi^N_I \rangle = \sum_{q,r,s} \langle \phi_{Elm} \phi_q | \hat{g} | \phi_r \phi_s \rangle \gamma^{IF}_{qsr}. \quad (14)$$

$\hat{a}^\dagger_{Elm}$ is the continuum creation operator, $\hat{h}$ is the one-electron Hamiltonian operator, $\hat{g}$ is the two-electron Coulomb operator, and $\{\phi_p, \phi_q, \ldots\}$ represents the set of spin orbitals. The one-particle Dyson orbital expansion coefficient γ^{IF}_p was already defined in Eq. (3). The two-particle Dyson matrix element γ^{IF}_{qsr} reads[8,47,50]

$$\gamma^{IF}_{qsr} = \langle \Psi^{N-1}_F | \hat{a}^\dagger_q \hat{a}_s \hat{a}_r | \Psi^N_I \rangle, \quad (15)$$

with $\hat{a}_s$ and $\hat{a}_r$ being fermionic annihilation operators with respect to the spin orbitals of the initial state wave function $|\Psi^N_I\rangle$, and $\hat{a}^\dagger_q$ creation operator with respect to the spin orbitals of the final state $|\Psi^{N-1}_F\rangle$ wave function. The resulting matrix elements are computed within the RASSI formalism[49,52] on the biorthonormal set of spin orbitals $\{\tilde{\phi}\}$.

In our approximation, the one-electron part in Eq. (12), that is, the $A_{IF;Elm}$ matrix elements, is neglected.[47] Thereby, Eq. (12) reduces to

$$\Gamma_{IF;Elm} = 2\pi |B_{FI;Elm}|^2, \quad (16)$$

with the two-electron matrix elements being approximated by pre-calculated bound-continuum atomic integrals from Ref. 65. For more details on our implementation of the OCA approximation to compute Auger decay rates, please refer to Tenorio et al.[47]

III. COMPUTATIONAL DETAILS

Initial core-ionized states and final decay states of Ar have been computed with the restricted active space self-consistent field

TABLE I. Number of roots computed with *ASI* for each irreducible representation of the D_{2h} point group symmetry for each final decay state.

Decaying state	A_g	B_{1g}	B_{2g}	B_{3g}	A_u	B_{1u}	B_{2u}	B_{3u}
$^1\mathrm{Ar}^{2+}$	220	160	160	160		180	180	180
$^3\mathrm{Ar}^{2+}$	280	210	210	210		270	270	270
$^2\mathrm{Ar}^{3+}$	300	300	300	300	300	300	300	300

(RASSCF) approach.[66] The restricted active space approach is based on a threefold division of the correlation orbital space, denoted RAS1, RAS2, and RAS3. The RASSCF calculations have been performed with two different selections of active spaces using the Douglas–Kroll basis set aug-cc-pCVQZ-DK,[67] further augmented with additional three s, three p, and two d Rydberg-type functions following the recipe proposed by Kaufmann, Baumeister, and Jungen.[68] The complete basis set is given in the supplementary material. Scalar relativistic effects have been taken into account by the Douglas–Kroll–Hess Hamiltonian up to second order in all the calculations.[69] Our results were obtained with the OpenMolcas program package.[53]

The first active space, named *ASI*, was formed with the $1s$ orbital in the RAS1 subspace, followed by the valence orbitals $2s$, $2p$, $3s$, and $3p$ in the RAS2 subspace, and the virtual $4s$, $4p$, and $5p$ in the RAS3 subspace. A maximum of one hole and one electron were allowed in RAS1 and RAS3, respectively. The second active space, named *ASII*, is similar to *ASI*, but with the addition of the virtual $5s$, $3d$, and $6p$ orbitals in RAS3. The RASSCF wave functions have been corrected by the multi-state restricted active space perturbation theory of second order (MS-RASPT2) approach.[70,71]

The final states of the Auger decay process were obtained by state averaging over a large number of roots for each irreducible representation of the D_{2h} point group. Notice that, in a purely atomic approach, the atomic orbitals are eigenstates of angular momentum operators.[72] On the other hand, our computational method does not exploit SO(3) symmetry and angular momentum expectation values, because it is mainly aimed at application to molecular systems.[53]

A major practical challenge in computing *KLL* AES spectra of third-row elements is to reach double cationic states with two holes in the inner valence L shell ($2s$ and $2p$), as the lowest lying double cationic states are the ones with ionized electrons from the M shell ($3s$ and $3p$). Moreover, the necessary number of roots grows exponentially when increasing the number of active orbitals, turning the computation of final decaying states of *KLL* Auger processes with *ASII* unpractical. Therefore, only *ASI* has been used to compute final states for Auger decay. The total number of roots calculated at each irreducible representation of the D_{2h} point group is given in Table I for each final decay state. Core-ionized states relevant to the XPS spectrum were obtained for 20 A_g states either with *ASI* or *ASII*.

## IV. RESULTS AND DISCUSSION

A. Ar $[1s^{-1}]$ XPS

In Table II, we present the calculated binding energies for singly charged core states having pole strengths larger than 10^{-4}, as

TABLE II. Calculated binding energies (BE) of core-ionized states of Argon, ΔBE relative to the primary ionization and square norms of the Dyson orbital (pole strengths R_I). We present results computed with the two active spaces *ASI* and *ASII* for which the pole strength is higher than 10^{-4}. Italicface denotes spurious states possibly introduced by the use of a very diffuse basis set.

Ionization character	*ASI*			*ASII*			Assignment
	BE (eV)	ΔBE (eV)	R_I	BE (eV)	ΔBE (eV)	R_I	
Primary	3207.82	0	0.7621	3207.90	0	0.7529	$[1s^{-1}]$
Shake-up	3231.21	23.39	0.0322	3231.22	23.32	0.0163	$[1s^{-1}3p^{-1}4p^1]$
Shake-up	*3232.20*	*24.38*	*0.0002*	*3231.26*	*23.36*	*0.0001*	$[1s^{-1}3p^{-1}4p^1]$
Shake-up	3232.15	24.33	0.0938	3232.26	24.36	0.0843	$[1s^{-1}3p^{-1}4p^1]$
Shake-up	*3235.43*	*27.61*	*0.0006*	*3235.42*	*27.51*	*0.0001*	$[1s^{-1}3s^{-1}5p^1]$
Shake-up	3236.43	28.44	0.0012	3235.49	27.58	0.0086	$[1s^{-1}3s^{-1}5p^1]$
Shake-up	3236.35	28.52	0.0010	3236.33	28.42	0.0051	$[1s^{-1}3s^{-1}5p^1]$
Shake-up				3237.69	29.79	0.0053	$[1s^{-1}3s^{-1}6p^1]$
Shake-up				3238.54	30.63	0.0031	$[1s^{-1}3s^{-1}6p^1]$
Shake-up	3244.99	37.17	0.0060	3245.75	37.85	0.0056	$[1s^{-1}3s^{-1}4s^1]$
Shake-up	3246.56	38.74	0.0041	3247.32	39.41	0.0036	$[1s^{-1}3s^{-1}4s^1]$
Shake-up				3251.46	43.56	0.0004	$[1s^{-1}3s^{-1}5s^1]$
Shake-up				3253.27	45.37	0.0002	$[1s^{-1}3s^{-1}5s^1]$
Shake-off	3240.40	32.51		3240.34	32.75		$[1s^{-1}3p^{-1}]$
Shake-off	3257.36	49.47		3257.33	49.74		$[1s^{-1}3s^{-1}]$

computed with the two active spaces *ASI* and *ASII*. Additionally, we also present the calculated binding energies of double ionized shake-off states $[1s^{-1}3p^{-1}]$ and $[1s^{-1}3s^{-1}]$. In Fig. 2, we plot the XPS spectrum obtained with *ASII*.

According to the LS coupling scheme, electronic configurations such as $[1s^{-1}3p^{-1}np^1]$, with two inequivalent *p* electrons (a hole $3p$ is the same as a single $3p$ electron) coupled with the unpaired spin of $1s$, can only result in two independent ^2S states. However, as shown
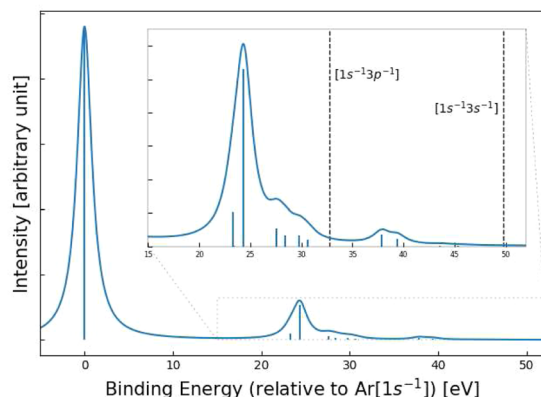
FIG. 2. Ar $[1s^{-1}]$ XPS computed at the RASPT2 level with *ASII*. The dashed lines represent the double ionization energies (shake-offs). The region between 15 and 50 eV is highlighted in the inset panel. The peaks have been broadened with Lorentzian functions using an arbitrarily chosen half width at half maximum (hwhm) parameter of 1.0 eV.

in Table II, we obtained more than two states with configurations $[1s^{-1}3p^{-1}4p^1]$ and $[1s^{-1}3p^{-1}5p^1]$ within a pole-strength threshold of 10^{-4}. While two of them are clearly the desired ^2S states, those with very low poles strengths are spurious states. Possible reasons for their occurrence could be the presence of very small exponents in the basis set used, or broken degeneracies introduced by the separate SCF optimizations. We noticed, for example, that if the XPS is computed using the regular aug-cc-pVQZ basis (see Table S2), no intruder states are obtained, i.e., only two $[1s^{-1}3p^{-1}np^1]$ states were generated. However, employing the regular aug-cc-pVQZ has the disadvantage of yielding inaccurate binding energies and intensities for the $1s^{-1}$ satellites of Argon. We briefly discuss the XPS results in the regular aug-cc-pVQZ basis in the supplementary material, Sec. S2.

Concerning the data shown in Table II, no significant changes have been observed for the binding energies obtained with both active spaces, except for contributions of $[1s^{-1}3p^{-1}6p^1]$ shake-up states that are absent in *ASI*, as this active space does not contain $6p$ orbitals. The binding energy of the primary peak was experimentally obtained as 3206.3 ± 0.3 eV,[34] which is ~1 eV below our calculated values. The relative binding energy (ΔE) of the intense shake-up peak $[1s^{-1}3p^{-1}4p^1]$ was obtained here around 24.4 eV, which is in excellent agreement with the experimentally measured binding energy[33] of 24 ± 0.5 eV, and with other calculations from Dyall[32] using the MCDF approach. Moreover, double ionized shake-off binding energies obtained here at around 32.5 and 49.5 eV for $[1s^{-1}3p^{-1}]$ and $[1s^{-1}3s^{-1}]$ are in good agreement with the values obtained in Ref. 25.

The relative intensities estimated from the ratio between the calculated peaks of $[1s^{-1}3p^{-1}4p^1]$ and $[1s^{-1}]$, are 13% and 12%,

for *ASI* and *ASII*, respectively, while the experimentally determined relative intensity was 10% ± 1%.[33] As shake-off states correspond to doubly charged species in their final states, we cannot provide a direct estimate for their intensities with the approximation employed here. However, we can propose an indirect estimate assuming that the sum of pole strengths of all final states should converge asymptotically to the total number of ionized electrons, i.e., to 1.

The sum of pole strengths of all singly ionized states was obtained as 0.88 with *ASI* and 0.90 with *ASII*. We then assume that what is missing to 1 (i.e., 100%) is related to doubly ionized shake-offs, that is, around 10%. The sum of the pole strengths of shake-ups was computed as 0.14 and 0.13 with *ASI* and *ASII*, respectively, of which ≈95% corresponds to the strongest $[1s^{-1}3p^{-1}4p^1]$ shake-up alone for both *ASI* and *ASII*. Therefore, to simulate the total Auger decay spectrum of Ar with a considerable excess of

FIG. 3. Ar *KLL* AES computed with *ASI* for the primary $[1s^{-1}]$, shake-up $[1s^{-1}3p^{-1}4p^1]$, and shake-off $[1s^{-1}3p^{-1}]$ initial states. Green and orange sticks come from, respectively, singlet and triplet decay channels of $[1s^{-1}]$. Purple and gray sticks come from decay channels of the shake-up and shake-off initial states $[1s^{-1}3p^{-1}4p^1]$, and $[1s^{-1}3p^{-1}]$, respectively. The calculated spectra have been shifted by −1.0 eV and broadened with Lorentzian functions using hwhm = 1.0 eV.

energy above the $[1s^{-1}]$ threshold, we can tentatively estimate the primary ionization to correspond approximately to 80% of the total Auger decay spectrum, followed by ≈10% of shake-up and ≈10% of shake-off. For simplicity, we assume only the $[1s^{-1}3p^{-1}4p^1]$ initial shake-up state for the Auger decay spectrum, since, according to our calculations, it contributes to ≈95% of the total shake-up intensity.

We also assumed that the $[1s^{-1}3s^{-1}]$ shake-off has a negligible contribution compared with the $[1s^{-1}3p^{-1}]$ shake-off. This was demonstrated, for example, in Ref. 25, where the probabilities of the shake-offs $[1s^{-1}3s^{-1}]$ and $[1s^{-1}3p^{-1}]$ were obtained as 3% and 16%, respectively, using relativistic multi-configuration calculations. In Sec. IV B, we will use our estimated populations of initial core-ionized states to scale the combined (total) KLL Auger spectrum of Argon.

Our populations are in fairly good agreement with previous theoretical and experimental studies that showed that satellite structures originating from valence orbitals are responsible for about 20% of the transitions that produce additional final states for the Auger decay.[25,35]
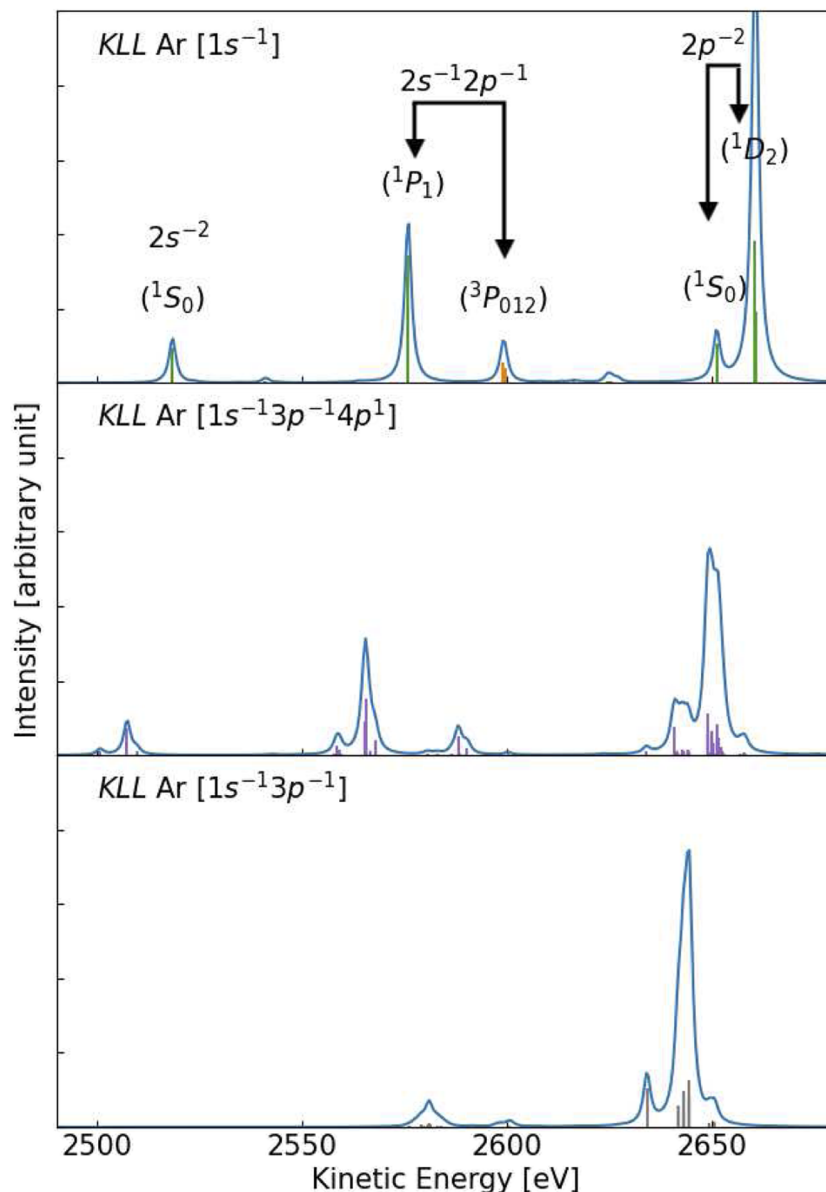
B. Ar KLL AES

The KLL AES computed with ASI for each of the primary ($[1s^{-1}]$), shake-up ($[1s^{-1}3p^{-1}4p^1]$), and shake-off ($[1s^{-1}3p^{-1}]$) initial states are shown in the three panels of Fig. 3. The simulated

spectra have been shifted by −1.0 eV and broadened with Lorentzian functions using a half width at half maximum (hwhm) parameter of 1.0 eV, to better compare with the experimental spectrum. The total decay rate of the primary ionization state has been obtained as 166.7×10^{-4} a.u. or 456 meV, which is in good agreement with other calculations,[23,73] as well as experimental data.[20,23] The values of the KLL partial decay rates of the primary ionization state are collected in Table III, where we also compare with *ab initio* results from Ref. 20. The corresponding kinetic energies computed for the primary ionization decay spectrum are 2519.36 eV ($^1S_0$), 2576.84 eV ($^1P_1$), 2600.45 eV ($^3P_{012}$), 2652.19 eV ($^1S_0$), and 2661.50 eV ($^1D_2$).

We also identify shake transitions in the KLL AES spectrum of Ar $[1s^{-1}]$ with calculated kinetic energies around 2625.5 eV. These transitions are associated with the decay process $[1s^{-1}] \rightarrow [2p^{-2}3p^{-1}4p^1]$. The 2600–2680 eV region of the Ar $[1s^{-1}]$ spectrum is highlighted in the supplementary material, Fig. S1, where the shake transitions can be better compared with primary decay states. We note that these transitions represent ~2% of the total decay rate of Ar $[1s^{-1}]$.

The Auger decay features of shake-up and shake-off initial states are listed in Table IV. A few lines associated with shake-up decay channels $[1s^{-1}3p^{-1}4p^1] \rightarrow [2p^{-2}3p^{-1}4p^1]$ accumulate intensity around 2652 ± 1 eV, which overlaps with the $^1S_0$ (2652.2 eV) decay channel of the primary ionization. Another prominent feature that is associated with the $[1s^{-1}3p^{-1}4p^1] \rightarrow [2s^{-1}2p^{-1}3p^{-1}4p^1]$ shake-up decay process is found at around 2566 eV. All these features initiated by a shake-up ionization are observed in the measured spectra of Ref. 31 obtained with photon energies of $h\nu$ = 4500 eV, although only spectral features with kinetic energy above 2600 eV have been previously assigned.

$[2p^{-2}3p^{-1}5p^1]$ decay states are generated by shake transitions during the Auger decay process of the shake-up ionization, but our calculations demonstrate that such transitions give negligible contributions to the total KLL Auger decay rate. In Ref. 31, the authors argue that configurations including 3d and 6p orbitals should be

TABLE III. Ar KLL AES partial decay rates for the primary ionization $[1s^{-1}]$ (in multiples of 10^{-4} a.u.).

Channel	$^1S_0$	$^1P_1$	$^3P_{012}$	$^1S_0$	$^1D_2$	Total
This work	10.3	35.5	9.6	11.9	98.8	166.7
Reference 20	13.6	35.2	8.4	8.10	102.5	170.8

TABLE IV. Auger decay features from the simulated KLL AES spectra of argon and ionization character assignment.

| Ionization character of initial state	Kinetic energy (eV)	Partial decay rates (×10^{-4} a.u.)	Assignment final state
Shake-up	2508.29	7.28	$[2s^{-2}3p^{-1}4p^1]$
Shake-up	2566.15	8.98	$[2s^{-1}2p^{-1}3p^{-1}4p^1]$
Shake-up	2566.60	15.28	$[2s^{-1}2p^{-1}3p^{-1}4p^1]$
Shake-up	2641.76	7.65	$[2p^{-2}3p^{-1}4p^1]$
Shake-up	2650.08	5.35	$[2p^{-2}3p^{-1}4p^1]$
Shake-up	2649.88	5.54	$[2p^{-2}3p^{-1}4p^1]$
Shake-up	2650.92	3.32	$[2p^{-2}3p^{-1}4p^1]$
Shake-up	2652.55	4.61	$[2p^{-2}3p^{-1}4p^1]$
Shake-up	2652.33	4.25	$[2p^{-2}3p^{-1}4p^1]$
Shake-off	2635.17	10.60	$[2p^{-2}3p^{-1}]$
Shake-off	2642.81	5.93	$[2p^{-2}3p^{-1}]$
Shake-off	2644.12	9.47	$[2p^{-2}3p^{-1}]$
Shake-off	2645.43	12.65	$[2p^{-2}3p^{-1}]$

11 July 2023 14:23:38
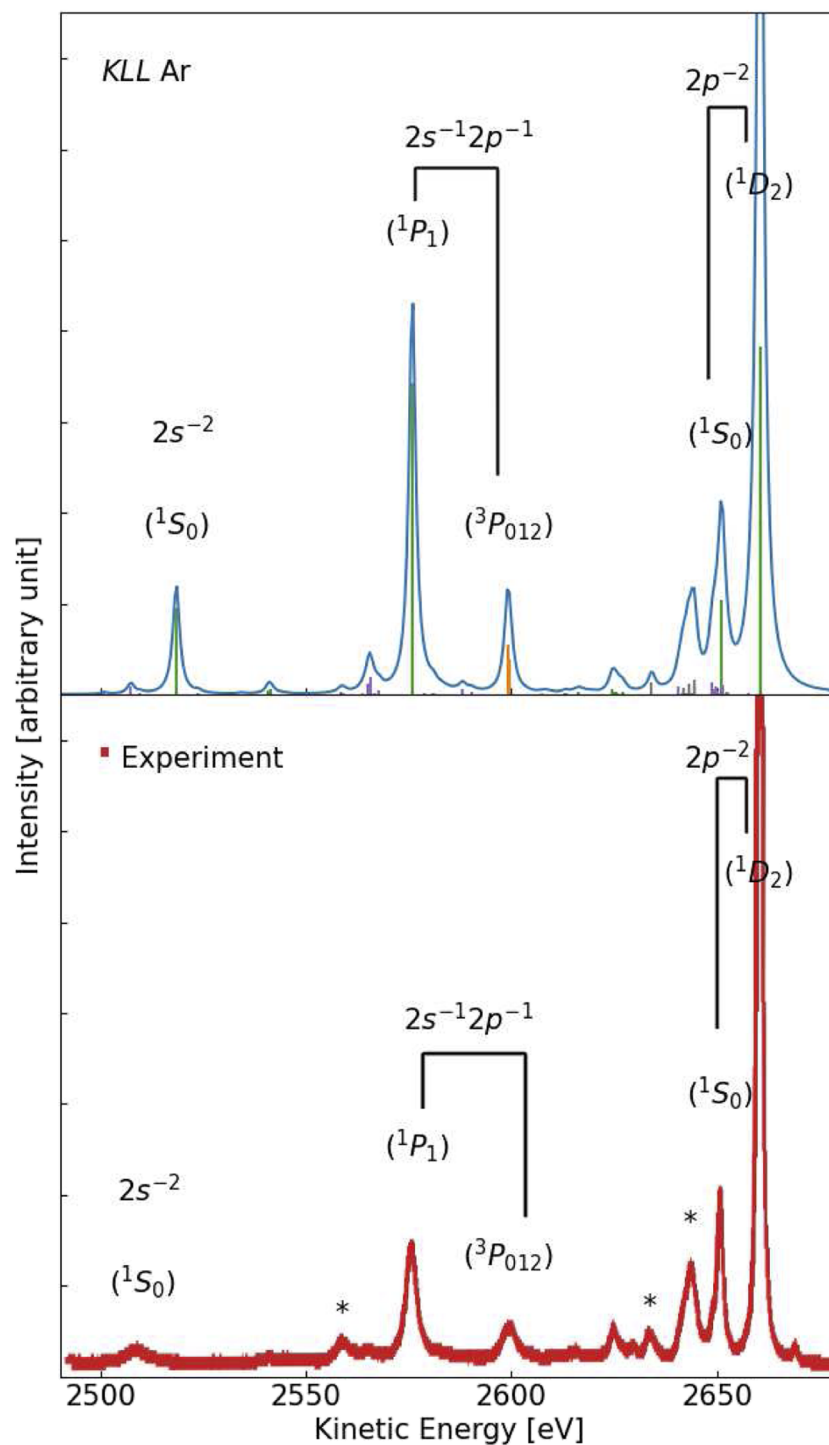
FIG. 4. Combined Ar *KLL* AES spectra scaled to 80% of primary, 10% of shake-up, and 10% of shake-off. The color code for the sticks in the top panel is the same as in Fig. 3. The calculated spectra were shifted by −1.0 eV and broadened with Lorentzian functions using hwhm = 1.0 eV. Experimental data (in red) measured with photon energy $h\nu$ = 4500 eV were digitized from Ref. 31. Peaks marked with a star in the experimental spectrum were associated with satellite initial states.

taken into account for an assignment of the shake features of the *KLL* AES spectrum of Argon. However, following our discussion on the satellite structure of the XPS spectrum, initial shake-up states involving the $6p$ and $3d$ orbitals would also be expected to have a minor contribution to the total intensity of the Auger decay spectrum, similar to what we observed for the $5p$ orbital.

The spectrum resulting from a shake-off $[1s^{-1}3p^{-1}]$ initial state is shown in the bottom panel of Fig. 3. The most intense peaks initiated by the shake-off show up at around 2644 ± 2 eV (see Table IV), where some of the shake-up peaks are also found. A single peak, here computed at 2635.2 eV, was also observed experimentally,[31] where it was also assigned to the $[1s^{-1}3p^{-1}] \rightarrow [2p^{-2}3p^{-1}]$ decay process.

All in all, our assignments of the shake features of the Auger decay spectrum agree with the ones from Ref. 31, which were mainly obtained from more simplistic fit analyses based on relativistic configuration interaction energies of the final states.

In Fig. 4, we combine the *KLL* AES computed for the primary ($[1s^{-1}]$), shake-up ($[1s^{-1}3p^{-1}4p^1]$), and shake-off ($[1s^{-1}3p^{-1}]$) initial states by scaling the intensities—that is the partial decay rates—of the corresponding spectra to 80%, 10%, and 10%, respectively, based on the arguments we presented in our discussion of the XPS spectrum. The experimental spectrum measured with photon energy $h\nu = 4500$ eV, digitized from Ref. 31, is plotted below the simulated spectrum, where features identified as originating from shake transitions are marked with a star. The scaled total decay rate of the combined spectrum is 166.13×10^{-4} a.u. or 452 meV, which is very similar to the total decay rate of the primary ionization.

Overall, our scaled simulated spectrum shows very good correspondence with most features of the experimental spectrum, except for the apparently overestimated intensities of the peaks due to the $2s^{-1}2p^{-1}$ and $2s^{-2}$ configurations, as compared with those of the $2p^{-2}$. Overestimated intensities associated with these peaks were also observed in previous theoretical studies,[20] and their cause remains unclear. We do not discard the possibility that the overestimation is linked to limitations in our calculations, such as correlation or insufficiently large active space. Nonetheless, the broadening of these peaks in the experimental spectrum suggests the dominance of other processes such as Coster–Kronig Auger effect,[74,75] resulting in the decay of an additional $3s$ or $3p$ valence electron filling the inner valence $2s$ hole. A fit analysis of the width of the experimental Ar $[1s^{-1}] \rightarrow [2s^{-2}]$ and $[1s^{-1}] \rightarrow [2s^{-1}2p^{-1}]$ peaks yielded lifetime broadenings of ~5.5 and 2.2 eV, respectively,[31] which are much larger than our computed value of 452 meV for the total decay rate. Such cascade Auger Coster–Kronig effects are not taken into account in our simulations, as they go beyond the scope of our study. We plan, however, an extension of the present study aiming at the Auger decay processes of double core hole species, such as Ar $[2s^{-2}]$.

The comparison between the simulated and the experimental spectra of Fig. 4 validates the use of the scaling factors of 80%, 10%, and 10% for primary and satellite initial states, obtained from the calculated XPS spectrum. The proposed protocol, as it relies only on *ab initio* results, can be used to disentangle the Auger spectrum of atoms and molecules[76] of other third-row elements, such as HCl, H_2S, PH_3, SO_2, SF_6, or SiH_4, in the vicinity of satellite states, which in many situations may be close-lying and/or overlapping with the primary ionization.

V. CONCLUSIONS

Accurate computations of argon's $[1s^{-1}]$ photoelectron spectrum and *KLL* AES spectra based on the RASPT2 level of theory were presented. The computed results were compared with recent state-of-the-art experimental data.[31] The Ar $[1s^{-1}]$ photoelectron spectrum was obtained with two active spaces, labeled *ASI* and *ASII*, where *ASI* includes all occupied plus the $4s$, $4p$, and $5p$ orbitals, while *ASII* extends *ASI* with the $5s$, $3d$, and $6p$ orbitals. The photoelectron spectra calculated with both active spaces demonstrated excellent agreement with previous theoretical studies and with experimental data.[31] The binding energies of the primary and satellite ionizations obtained with both *ASI* and *ASII* differ in most cases by less than 0.1 eV. We have identified shake transitions in the *KLL* AES spectrum of Ar $[1s^{-1}]$ associated with the decay process $[1s^{-1}] \rightarrow [2p^{-2}3p^{-1}4p^1]$. These shake transitions were found to represent ~2% of the total decay rate of the Auger spectrum of Ar $[1s^{-1}]$. Furthermore, the calculated intensities of the photoelectron spectrum were used to estimate the probabilities associated with the initial states on the subsequent *KLL* Auger decay, considering a measurement performed with photon energy around 50 eV above the Ar $[1s^{-1}]$ threshold. We estimated 80% of primary and 20% of satellite initial states, of which 10% are shake-up and 10% are shake-off. For the computation of the total combined Ar *KLL* Auger decay spectrum, we considered only the most intense $[1s^{-1}3p^{-1}4p^1]$ shake-up and the $[1s^{-1}3p^{-1}]$ double ionized shake-off state. Comparison of the simulated *KLL* AES with the experimental spectrum, obtained with photon energy $h\nu = 4500$ eV, showed that our estimated initial-state probabilities are capable of reproducing the main experimental features fairly well. Moreover, the assignments of the satellite features resulting from our calculations agree with the ones from Ref. 31, which are mostly based on the calculated energies of the final states. The proposed protocol can be further extended to probe the relaxation dynamics of different atoms and molecules in the presence of satellite states, providing significant insights into the electronic structure of complex systems.

SUPPLEMENTARY MATERIAL

The supplementary material contains: the computed spectra, the Rydberg-augmented basis set (Table S1), the binding energies computed with the *ASI* active space and the aug-cc-pVQZ basis set (Table S2), and the 2600–2680 eV region of the Ar $[1s^{-1}]$ spectrum (Fig. S1).

ACKNOWLEDGMENTS

AUTHOR DECLARATIONS

Conflict of Interest

The authors have no conflicts to disclose.

Author Contributions

Jacob Pedersen: Data curation (equal); Formal analysis (equal); Investigation (equal); Methodology (equal); Validation (equal); Visualization (equal); Writing – original draft (equal); Writing – review & editing (equal). **Piero Decleva**: Data curation (equal); Formal analysis (equal); Investigation (equal); Methodology (equal); Validation (equal); Writing – review & editing (equal). **Sonia Coriani**: Data curation (equal); Formal analysis (equal); Funding acquisition (equal); Investigation (equal); Methodology (equal); Project administration (equal); Resources (equal); Supervision (equal); Validation (equal); Writing – review & editing (equal). **Bruno Nunes Cabral Tenorio**: Conceptualization (lead); Data curation (equal); Formal analysis (equal); Funding acquisition (equal); Investigation (equal); Methodology (equal); Project administration (equal); Resources (equal); Software (equal); Validation (equal); Writing – original draft (lead); Writing – review & editing (equal).

DATA AVAILABILITY

The data that support the findings of this study are available within the article and its supplementary material.

REFERENCES

[1] D. Matsakis, A. Coster, B. Laster, and R. Sime, "A renaming proposal: 'The Auger–Meitner effect,'" Phys. Today **72**(9), 10 (2019).

[2] S. Svensson, "Soft x-ray photoionization of atoms and molecules," J. Phys. B: At., Mol. Opt. Phys. **38**, S821–S838 (2005).

[3] M. N. Piancastelli, T. Marchenko, R. Guillemin, L. Journel, O. Travnikova, I. Ismail, and M. Simon, "Hard x-ray spectroscopy and dynamics of isolated atoms and molecules: A review," Rep. Prog. Phys. **83**, 016401 (2019).

[4] J. Pedersen, M. H. Rasmussen, and K. V. Mikkelsen, "Redfield propagation of photoinduced electron transfer reactions in vacuum and solution," J. Chem. Theory Comput. **18**, 7052–7072 (2022).

[5] D. Gust, T. A. Moore, and A. L. Moore, "Solar fuels via artificial photosynthesis," Acc. Chem. Res. **42**, 1890–1898 (2009).

[6] C. A. Rozzi, S. M. Falke, N. Spallanzani, A. Rubio, E. Molinari, D. Brida, M. Maiuri, G. Cerullo, H. Schramm, J. Christoffers, and C. Lienau, "Quantum coherence controls the charge separation in a prototypical artificial light-harvesting system," Nat. Commun. **4**, 1602 (2013).

[7] A. Monti, H. J. M. de Groot, and F. Buda, "*In silico* design of a donor–antenna–acceptor supramolecular complex for photoinduced charge separation," J. Phys. Chem. C **118**, 15600–15609 (2014).

[8] B. N. C. Tenorio, K. B. Møller, P. Decleva, and S. Coriani, "Disentangling the resonant Auger spectra of ozone: Overlapping core-hole states and core-excited state dynamics," Phys. Chem. Chem. Phys. **24**, 28150–28163 (2022).

[9] A. Hans, P. Schmidt, C. Küstner-Wetekam, F. Trinter, S. Deinert, D. Bloß, J. H. Viehmann, R. Schaf, M. Gerstel, C. M. Saak, J. Buck, S. Klumpp, G. Hartmann, L. S. Cederbaum, N. V. Kryzhevoi, and A. Knie, "Suppression of x-ray-induced radiation damage to biomolecules in aqueous environments by immediate intermolecular decay of inner-shell vacancies," J. Phys. Chem. Lett. **12**, 7146–7150 (2021).

[10] L. H. Coutinho, F. de A. Ribeiro, B. N. C. Tenorio, S. Coriani, A. C. F. dos Santos, C. Nicolas, A. R. Milosavljevic, J. D. Bozek, and W. Wolff, "NEXAFS and MS-AES spectroscopy of the C 1s and Cl 2p excitation and ionization of chlorobenzene: Production of dicationic species," Phys. Chem. Chem. Phys. **23**, 27484–27497 (2021).

[11] L. Inhester, B. Oostenrijk, M. Patanen, E. Kokkonen, S. H. Southworth, C. Bostedt, O. Travnikova, T. Marchenko, S.-K. Son, R. Santra, M. Simon, L. Young, and S. L. Sorensen, "Chemical understanding of the limited site-specificity in molecular inner-shell photofragmentation," J. Phys. Chem. Lett. **9**, 1156–1163 (2018).

[12] P. Bolognesi, J. A. Kettunen, A. Cartoni, R. Richter, S. Tosic, S. Maclot, P. Rousseau, R. Delaunay, and L. Avaldi, "Site-and state-selected photofragmentation of 2Br-pyrimidine," Phys. Chem. Chem. Phys. **17**, 24063–24069 (2015).

[13] Y.-J. Chiang, Y.-S. Lin, H.-R. Lin, and C.-L. Liu, "Specific dissociation of core-excited pyrimidine nucleobases," Chem. Phys. Lett. **706**, 215–222 (2018).

[14] A. Ponzi, C. Angeli, R. Cimiraglia, S. Coriani, and P. Decleva, "Dynamical photoionization observables of the CS molecule: The role of electron correlation," J. Chem. Phys. **140**, 204304 (2014).

[15] R. L. Martin and D. A. Shirley, "Theory of the neon 1s correlation-peak intensities," Phys. Rev. A **13**, 1475–1483 (1976).

[16] L. S. Cederbaum and W. Domcke, "Theoretical aspects of ionization potentials and photoelectron spectroscopy: A Green's function approach," in *Advances in Chemical Physics* (John Wiley & Sons, Ltd., 1977), pp. 205–344.

[17] P. A. Heimann, D. W. Lindle, T. A. Ferrett, S. H. Liu, L. J. Medhurst, M. N. Piancastelli, D. A. Shirley, U. Becker, H. G. Kerkhoff, B. Langer, D. Szostak, and R. Wehlitz, "Shake-off on inner-shell resonances of Ar, Kr, and Xe," J. Phys. B: At. Mol. Phys. **20**, 5005 (1987).

[18] H. Aksela, S. Aksela, H. Pulkkinen, G. M. Bancroft, and K. H. Tan, "Anomalously strong shake-up processes in Auger decay of the resonantly excited $2p^53s^23p^6$ nl states of Ar," Phys. Rev. A **37**, 1798 (1988).

[19] G. Goldsztejn, R. Püttner, L. Journel, R. Guillemin, O. Travnikova, R. K. Kushawaha, B. Cunha de Miranda, I. Ismail, D. Céolin, M. N. Piancastelli, M. Simon, and T. Marchenko, "Electronic-state–lifetime interference in the hard-x-ray regime: Argon as a showcase," Phys. Rev. A **95**, 012509 (2017).

[20] J. Vayrynen, R. N. Sodhi, and R. G. Cavell, "Energies and intensities of the KLL Auger spectra of SiH_4, PH_3, HCl, and Ar," J. Chem. Phys. **79**, 5329–5336 (1983).

[21] T. A. Carlson and C. W. Nestor, Jr., "Calculation of electron shake-off probabilities as the result of X-ray photoionization of the rare gases," Phys. Rev. A **8**, 2887 (1973).

[22] R. Püttner, Y. Li, J. Zeng, D. Koulentianos, T. Marchenko, R. Guillemin, L. Journel, O. Travnikova, M. Zmerli, D. Céolin, Y. Azuma, S. Kosugi, M. N. Piancastelli, and M. Simon, "Argon $1s^{-2}$ Auger hypersatellites," J. Phys. B: At., Mol. Opt. Phys. **54**, 024001 (2020).

[23] L. Asplund, P. Kelfve, B. Blomster, H. Siegbahn, and K. Siegbahn, "Argon KLL and KLM Auger electron spectra," Phys. Scr. **16**, 268 (1977).

[24] M. Nakano, Y. Hikosaka, P. Lablanquie, F. Penent, S.-M. Huttula, I. Suzuki, K. Soejima, N. Kouchi, and K. Ito, "Auger decay of Ar 2p satellite states studied with a multielectron coincidence method," Phys. Rev. A **85**, 043405 (2012).

[25] J.-C. Dousse and J. Hoszowska, "L- and M-shell-electron shake processes following 1s photoionization in argon and krypton," Phys. Rev. A **56**, 4517–4531 (1997).

[26] T. A. Carlson and M. O. Krause, "Atomic readjustment to vacancies in the K and L shells of argon," Phys. Rev. **137**, A1655 (1965).

[27] T. Åberg, "Theory of x-ray satellites," Phys. Rev. **156**, 35–41 (1967).

[28] M. Žitnik, R. Püttner, G. Goldsztejn, K. Bučar, A. Mihelič, T. Marchenko, R. Guillemin, L. Journel, O. Travnikova, D. Céolin, M. N. Piancastelli, and M. Simon, "Two-to-one Auger decay of a double L vacancy in argon," Phys. Rev. A **93**, 021401(R) (2016).

[29] R. Guillemin, S. Sheinerman, R. Püttner, T. Marchenko, G. Goldsztejn, L. Journel, R. K. Kushawaha, D. Céolin, M. N. Piancastelli, and M. Simon, "Postcollision interaction effects in KLL Auger spectra following argon 1s photoionization," Phys. Rev. A **92**, 012503 (2015).

[30] R. Guillemin, K. Jänkälä, B. C. de Miranda, T. Marin, L. Journel, T. Marchenko, O. Travnikova, G. Goldsztejn, I. Ismail, R. Püttner, D. Céolin, B. Lassalle-Kaiser, M. N. Piancastelli, and M. Simon, "Interplay of complex decay processes after argon 1s ionization," Phys. Rev. A **97**, 013418 (2018).

[31] R. Püttner, P. Holzhey, M. Hrast, M. Žitnik, G. Goldsztejn, T. Marchenko, R. Guillemin, L. Journel, D. Koulentianos, O. Travnikova, M. Zmerli, D. Céolin, Y. Azuma, S. Kosugi, A. F. Lago, M. N. Piancastelli, and M. Simon, "Argon *KLL* Auger spectrum: Initial states, core-hole lifetimes, shake, and knock-down processes," Phys. Rev. A **102**, 052832 (2020).

[32] K. G. Dyall, "Shake theory predictions of excited-state populations following 1*s* ionisation in argon," J. Phys. B: At. Mol. Phys. **16**, 3137 (1983).

[33] S. H. Southworth, T. LeBrun, Y. Azuma, and K. G. Dyall, "Argon *KM* photoelectron satellites," J. Electron Spectrosc. Relat. Phenom. **94**, 33–38 (1998).

[34] M. Breinig, M. H. Chen, G. E. Ice, F. Parente, B. Crasemann, and G. S. Brown, "Atomic inner-shell level energies determined by absorption spectrometry with synchrotron radiation," Phys. Rev. A **22**, 520–528 (1980).

[35] G. B. Armen, T. Åberg, K. R. Karim, J. C. Levin, B. Crasemann, G. S. Brown, M. H. Chen, and G. E. Ice, "Threshold double photoexcitation of argon with synchrotron radiation," Phys. Rev. Lett. **54**, 182–185 (1985).

[36] B. N. C. Tenorio, S. Coriani, A. B. Rocha, and M. A. C. Nascimento, "Molecular photoionization and photodetachment cross sections based on L^2 basis sets: Theory and selected examples," in *Advances in Methods and Applications of Quantum Systems in Chemistry, Physics, and Biology*, edited by A. V. Glushkov, O. Y. Khetselius, J. Maruani, and E. Brändas (Springer International Publishing, Cham, 2021), pp. 151–179.

[37] B. N. C. Tenorio, M. A. C. Nascimento, S. Coriani, and A. B. Rocha, "Coupled cluster study of photoionization and photodetachment cross sections," J. Chem. Theory Comput. **12**, 4440–4459 (2016).

[38] B. N. C. Tenorio, M. A. C. Nascimento, A. B. Rocha, and S. Coriani, "Lanczos-based equation-of-motion coupled-cluster singles-and-doubles approach to the total photoionization cross section of valence excited states," J. Chem. Phys. **151**, 184106 (2019).

[39] T. Moitra, A. Ponzi, H. Koch, S. Coriani, and P. Decleva, "Accurate description of photoionization dynamical parameters," J. Phys. Chem. Lett. **11**, 5330–5337 (2020).

[40] T. Moitra, S. Coriani, and P. Decleva, "Capturing correlation effects on photoionization dynamics," J. Chem. Theory Comput. **17**, 5064–5079 (2021).

[41] W. Skomorowski and A. I. Krylov, "Feshbach–Fano approach for calculation of Auger decay rates using equation-of-motion coupled-cluster wave functions. I. Theory and implementation," J. Chem. Phys. **154**, 084124 (2021).

[42] L. Inhester, C. F. Burmeister, G. Groenhof, and H. Grubmüller, "Auger spectrum of a water molecule after single and double core ionization," J. Chem. Phys. **136**, 144304 (2012).

[43] G. Grell, O. Kühn, and S. I. Bokarev, "Multireference quantum chemistry protocol for simulating autoionization spectra: Test of ionization continuum models for the neon atom," Phys. Rev. A **100**, 042512 (2019).

[44] G. Grell and S. I. Bokarev, "Multi-reference protocol for (auto)ionization spectra: Application to molecules," J. Chem. Phys. **152**, 074108 (2020).

[45] F. Matz and T.-C. Jagau, "Molecular Auger decay rates from complex-variable coupled-cluster theory," J. Chem. Phys. **156**, 114117 (2022).

[46] P. Decleva, M. Stener, and D. Toffoli, "Continuum electronic states: The Tiresia code," Molecules **27**, 2026 (2022).

[47] B. N. C. Tenorio, T. A. Voß, S. I. Bokarev, P. Decleva, and S. Coriani, "Multireference approach to normal and resonant Auger spectra based on the one-center approximation," J. Chem. Theory Comput. **18**, 4387–4407 (2022).

[48] A. K. Schnack-Petersen, B. N. C. Tenorio, S. Coriani, P. Decleva, J. Troß, K. Ramasesha, M. Coreno, R. Totani, and A. Röder, "Core spectroscopy of oxazole," J. Chem. Phys. **157**, 214305 (2022).

[49] P.-Å. Malmqvist and B. O. Roos, "The CASSCF state interaction method," Chem. Phys. Lett. **155**, 189–194 (1989).

[50] B. N. C. Tenorio, P. Decleva, and S. Coriani, "Multi-reference approach to the computation of double core-hole spectra," J. Chem. Phys. **155**, 131101 (2021).

[51] B. N. C. Tenorio, A. Ponzi, S. Coriani, and P. Decleva, "Photoionization observables from multi-reference Dyson orbitals coupled to B-spline DFT and TD-DFT continuum," Molecules **27**, 1203 (2022).

[52] P. Å. Malmqvist, "Calculation of transition density matrices by nonunitary orbital transformations," Int. J. Quantum Chem. **30**, 479–494 (1986).

[53] G. L. Manni, I. F. Galván, A. Alavi, F. Aleotti, F. Aquilante, J. Autschbach, D. Avagliano, A. Baiardi, J. J. Bao, S. Battaglia, L. Birnoschi, A. Blanco-González, S. I. Bokarev, R. Broer, R. Cacciari, P. B. Calio, R. K. Carlson, R. Carvalho Couto, L. Cerdán, L. F. Chibotaru, N. F. Chilton, J. R. Church, I. Conti, S. Coriani, J. Cuéllar-Zuquin, R. E. Daoud, N. Dattani, P. Decleva, C. de Graaf, M. G. Delcey, L. D. Vico, W. Dobrautz, S. S. Dong, R. Feng, N. Ferré, M. Filatov(Gulak), L. Gagliardi, M. Garavelli, L. González, Y. Guan, M. Guo, M. R. Hennefarth, M. R. Hermes, C. E. Hoyer, M. Huix-Rotllant, V. K. Jaiswal, A. Kaiser, D. S. Kaliakin, M. Khamesian, D. S. King, V. Kochetov, M. Krośnicki, A. A. Kumaar, E. D. Larsson, S. Lehtola, M.-B. Lepetit, H. Lischka, P. López Ríos, M. Lundberg, D. Ma, S. Mai, P. Marquetand, I. C. D. Merritt, F. Montorsi, M. Mörchen, A. Nenov, V. H. A. Nguyen, Y. Nishimoto, M. S. Oakley, M. Olivucci, M. Oppel, D. Padula, R. Pandharkar, Q. M. Phung, F. Plasser, G. Raggi, E. Rebolini, M. Reiher, I. Rivalta, D. Roca-Sanjuán, T. Romig, A. A. Safari, A. Sánchez-Mansilla, A. M. Sand, I. Schapiro, T. R. Scott, J. Segarra-Martí, F. Segatta, D.-C. Sergentu, P. Sharma, R. Shepard, Y. Shu, J. K. Staab, T. P. Straatsma, L. K. Sørensen, B. N. C. Tenorio, D. G. Truhlar, L. Ungur, M. Vacher, V. Veryazov, T. A. Voss, O. Weser, D. Wu, X. Yang, D. Yarkony, C. Zhou, J. P. Zobel, and R. Lindh, "The OpenMolcas web: A community-driven approach to advancing computational chemistry," J. Chem. Theory Comput. (published online, 2023).

[54] R. Arneberg, J. Müller, and R. Manne, "Configuration interaction calculations of satellite structure in photoelectron spectra of H$_2$O," Chem. Phys. **64**, 249–258 (1982).

[55] R. L. Martin and D. A. Shirley, "Theory of core-level photoemission correlation state spectra," J. Chem. Phys. **64**, 3685–3689 (1976).

[56] O. Goscinski and P. Lindner, "Natural spin-orbitals and generalized overlap amplitudes," J. Math. Phys. **11**, 1313–1317 (1970).

[57] C. M. Oana and A. I. Krylov, "Dyson orbitals for ionization from the ground and electronically excited states within equation-of-motion coupled-cluster formalism: Theory, implementation, and examples," J. Chem. Phys. **127**, 234106 (2007).

[58] J. V. Ortiz, "Dyson-orbital concepts for description of electrons in molecules," J. Chem. Phys. **153**, 070902 (2020).

[59] A. I. Krylov, "From orbitals to observables and back," J. Chem. Phys. **153**, 080901 (2020).

[60] M. Stener, S. Furlan, and P. Decleva, "Density functional calculations of photoionization with an exchange-correlation potential with the correct asymptotic behaviour," J. Phys. B: At., Mol. Opt. Phys. **33**, 1081 (2000).

[61] F. Lever, D. Mayer, J. Metje, S. Alisauskas, F. Calegari, S. Düsterer, R. Feifel, M. Niebuhr, B. Manschwetus, M. Kuhlmann, T. Mazza, M. S. Robinson, R. J. Squibb, A. Trabattoni, M. Wallner, T. J. A. Wolf, and M. Gühr, "Core-level spectroscopy of 2-thiouracil at the sulfur L$_1$- and L$_{2,3}$-edges utilizing a SASE free-electron laser," Molecules **26**, 6469 (2021).

[62] G. Wentzel, "Über strahlungslose quantensprünge," Z. Phys. **43**, 524–530 (1927).

[63] R. Manne and T. Åberg, "Koopmans' theorem for inner-shell ionization," Chem. Phys. Lett. **7**, 282–284 (1970).

[64] R. Manne and H. Ågren, "Auger transition amplitudes from general many-electron wavefunctions," Chem. Phys. **93**, 201–208 (1985).

[65] E. J. McGuire, "*K*-shell Auger transition rates and fluorescence yields for elements Be–Ar," Phys. Rev. **185**, 1–6 (1969).

[66] J. Olsen, B. O. Roos, P. Jørgensen, and H. J. A. Jensen, "Determinant based configuration interaction algorithms for complete and restricted configuration interaction spaces," J. Chem. Phys. **89**, 2185–2192 (1988).

[67] D. E. Woon and T. H. Dunning, "Gaussian basis sets for use in correlated molecular calculations. IV. Calculation of static electrical response properties," J. Chem. Phys. **100**, 2975–2988 (1994).

[68] K. Kaufmann, W. Baumeister, and M. Jungen, "Universal Gaussian basis sets for an optimum representation of Rydberg and continuum wavefunctions," J. Phys. B: At., Mol. Opt. Phys. **22**, 2223–2240 (1989).

[69] T. Nakajima and K. Hirao, "The Douglas-Kroll-Hess approach," Chem. Rev. **112**, 385–402 (2012).

[70] P. Å. Malmqvist, K. Pierloot, A. R. M. Shahi, C. J. Cramer, and L. Gagliardi, "The restricted active space followed by second-order perturbation theory method: Theory and application to the study of CuO$_2$ and Cu$_2$O$_2$ systems," J. Chem. Phys. **128**, 204109 (2008).

[71] V. Sauri, L. Serrano-Andrés, A. R. M. Shahi, L. Gagliardi, S. Vancoillie, and K. Pierloot, "Multiconfigurational second-order perturbation theory restricted active space (RASPT2) method for electronic excited states: A benchmark study," J. Chem. Theory Comput. **7**, 153–168 (2011).

[72] K. G. Dyall, I. P. Grant, C. T. Johnson, F. A. Parpia, and E. P. Plummer, "GRASP: A general-purpose relativistic atomic structure program," Comput. Phys. Commun. **55**, 425–456 (1989).

[73] M. H. Chen and B. Crasemann, "K–LL Auger transition probabilities for elements with low and intermediate atomic numbers," Phys. Rev. A **8**, 7–13 (1973).

[74] R. Feifel, J. H. D. Eland, R. J. Squibb, M. Mucke, S. Zagorodskikh, P. Linusson, F. Tarantelli, P. Kolorenč, and V. Averbukh, "Ultrafast molecular three-electron Auger decay," Phys. Rev. Lett. **116**, 073001 (2016).

[75] P. Lablanquie, F. Penent, R. I. Hall, H. Kjeldsen, J. H. D. Eland, A. Muehleisen, P. Pelicon, ž. šmit, M. žitnik, and F. Koike, "Coster-Kronig decay of the Ar $2s$ hole observed by Auger-threshold photoelectron coincidence spectroscopy," Phys. Rev. Lett. **84**, 47–50 (2000).

[76] R. Püttner, D. Céolin, R. Guillemin, R. K. Kushawaha, T. Marchenko, L. Journel, M. N. Piancastelli, and M. Simon, "Detailed analysis of shake structures in the KLL Auger spectrum of H_2S," Phys. Rev. A **93**, 042501 (2016).

11 July 2023 14:23:38